Catalysis Today 166 (2011) 180–187

Contents lists available at ScienceDirect

Catalysis Today

journal homepage: www.elsevier.com/locate/cattod

Enhancement of catalytic wet air oxidation of tert-amyl methyl ether by the addition of Sn and CeO_2 to Rh/Al_2O_3 catalysts

I. Cuauhtémoc[a], G. Del Angel[a,*], G. Torres[b], C. Angeles-Chavez[c], J. Navarrete[c], J.M. Padilla[a]

[a] Universidad Autónoma Metropolitana-Iztapalapa, Laboratorio de Catálisis, Departamento de Química, DCBI, Av. San Rafael Atlixco No. 186, CP 09340, México DF, Mexico
[b] Universidad Juárez Autónoma de Tabasco, Laboratorio de catálisis heterogénea, Área de Química, DACB, Km.-1 carretera Cunduacán-Jalpa de Méndez AP. 24, C.P. 86690, Cunduacán Tabasco, Mexico
[c] Instituto Mexicano del Petróleo, Programa de Ingenieria Molecular, Eje Central Lázaro Cárdenas 152, 07730 México DF, Mexico

ARTICLE INFO

Article history:
Available online 8 February 2011

Keywords:
Catalytic wet air oxidation
Tert-amyl-methyl ether (TAME)
Rh/alumina-ceria
Rh–Sn/alumina-ceria
XPS
FTIR-CO
TPR-H_2

ABSTRACT

The Rh and Rh–Sn supported catalyst on γ-Al_2O_3 and γ-Al_2O_3–CeO_2 (loading 1, 5 and 20 Ce wt%) were characterized by means of electron microscopy (TEM), temperature programmed reduction (TPR), Fourier transformed infrared of CO adsorption (FTIR-CO) and X-ray photoelectron spectroscopy (XPS). The catalysts were tested in the catalytic wet air oxidation of an aqueous solution of 227 ppm of TAME and 1 g/L of catalyst (120 °C and 10 bar of oxygen partial pressure). The rhodium monometallic catalysts showed an increase in the activity with the load of cerium oxide in the catalyst. The coexistence of $Rh^{\circ}/Rh^{\delta+}$ and Ce^{4+}/Ce^{3+} redox couples facilitates the activation of TAME and hence the catalytic activity and selectivity to mineralization. The addition of $Sn^{\delta+}$ enhances the activity and selectivity; this is explained by assuming that $Sn^{\delta+}$ acts as Lewis acid sites trapping the TAME molecules for further oxidation on rhodium metal particles.

1. Introduction

The tert-amyl methyl ether (TAME) and other ethers have been used as oxygenated additives of gasoline with the aim to increase the octane number and prevent the formation of COx, NOx and hence of ozone in the atmosphere [1]. However, due to the chemical properties of these compounds they were also found as important pollutants of the groundwater and as a consequence, during the last decades, important studies for the removal of pollutants in liquid phase have been investigated. Catalytic wet air oxidation (CWAO) has been used in recent times for the total oxidation of a great diversity of pollutants in water [2–4]. Of particular interest was the development of effective catalysts containing noble metals which are able to attain higher activity and great selectivity, Ru, Rh, Pt, Pd and Ag supported on Al_2O_3, SiO_2, TiO_2, graphite, ZrO_2, CeO_2, etc. have proved to be reactive towards the wet oxidation on phenols [5,6], dyes [7], carboxylic acids [8–10] ammonia [11], aniline [12], butyric acid [13], oleic acid [14], and acetic acid [15] among others. On the other hand, the addition of a second active metal of group IV (Ge, Sn or Pb) to Pt, Pd, Rh or Ru has shown to be selective for several chemical processes as an example for hydrogenation or hydrogenolysis reactions [16,17]. In many studies it appears that the second metal as Sn remains as cationic species after reduction associated with the noble metal as Pt and Rh [18,19], modifying the noble metal properties by either geometric or electronic effects. In addition, the Al_2O_3–CeO_2 support has been reported as efficient for the oxidation of organic compounds [20]. Its performance comes from the formation of Ce^{3+}/Ce^{4+} pair, since the oxidation and reduction cycles are important for the storage and oxygen supply during the oxidation of organic compounds. For the CH_4/CO_2 reforming reaction it has been reported that CeO_2 promotes the Rh activity, the beneficial effects of CeO_2 might have occurred either because the cooperative between the partial CeO_x and Rh have generated sites with higher activity, or because the oxidative properties of CeO_2 increased the dissociation of CO_2 [21,22].

In the present work the oxidative properties of Rh/Al_2O_3–CeO_2 and Rh–Sn/Al_2O_3–CeO_2 catalysts on the catalytic wet air oxidation of tert-amyl methyl ether were studied. The supports were prepared by incorporating cerium nitrate (1, 5 and 20 wt% of Ce) with boehmite (Catapl B). The catalysts were characterized by transmission electron microscopy (TEM), CO adsorption followed by Fourier transmission infrared spectroscopy (FTIR-CO), X-ray photoelectron spectroscopy (XPS) and temperature programmed reduction of hydrogen (TPR-H_2). The activity and selectivity towards the mineralization was evaluated by catalytic wet air oxidation of TAME.

* Corresponding author. Tel.: +52 55 58044668; fax: +52 55 58044666.
E-mail addresses: gdam@xanum.uam.mx, gloria.del.angel@hotmail.com (G. Del Angel).

0920-5861/$ – see front matter © 2011 Elsevier B.V. All rights reserved.
doi:10.1016/j.cattod.2010.11.100

Our aim was to find out relations between the structure, chemical state of the catalysts and the activity and selectivity towards mineralization.

2. Experimental

2.1. Catalysts

The γ-Al_2O_3 support was obtained by calcination of the boehmite Catapal B (CONDEA, high purity 99.999%, 74% AlOOH, 26% H_2O) under air flow (3.6 L/min) at 650 °C for 12 h. The γ-alumina-ceria supports containing 1, 5 and 20 Ce wt%, were prepared by adding the appropriated amounts of aqueous solution containing $Ce(NO_3)_3{\cdot}6H_2O$ (Strem Chemicals, 99.9%) to the aluminum boehmite Catapal B. Afterwards, the impregnated boehmite was kept under stirring in a rotary evaporator for 4 h. The water excess was evaporated under vacuum at 60 °C and then the solid was dried completely in an oven at 120 °C for 12 h. Finally, the γ-Al_2O_3–CeO_2 supports were obtained by annealing the samples under air flow at 650 °C for 24 h.

The Rh supported catalysts were prepared by wet impregnation of γ-Al_2O_3 and γ-Al_2O_3–Ce adding the appropriated amounts of an aqueous solution containing $RhCl_3{\cdot}3H_2O$ (Strem Chemicals 99.99%) to obtain a nominal concentration of 1 wt% of Rh. The Rh–Sn catalysts were prepared by the coimpregnation of γ-Al_2O_3 and γ-Al_2O_3–CeO_2 supports by adding the appropriated amounts of aqueous solutions containing $RhCl_3{\cdot}3H_2O$ or $SnCl_4{\cdot}H_2O$ (Strem Chemicals 99.99%) to obtain a nominal concentration of 1 wt% of Rh and 1.15 wt%Sn (molar ratio Rh/Sn = 1). The impregnated catalysts were dried at 120 °C in an oven for 12 h and then calcined under air flow (3.6 L/h) at 500 °C for 4 h. Finally, the catalysts were reduced at 500 °C under hydrogen flow (3.6 L/h) for 5 h and stored until characterization. The final percentage of Rh and Sn on the catalysts was obtained by Inductively Coupled Plasma Atomic Emission Spectrometry (ICP-AES). The catalysts containing CeO_2 were labeled as Rh/ACe*X* and Rh–Sn/ACe*X*, where A indicates alumina, *X* the Ce amount for each sample, *X* = 1, 5, and 20 wt%.

2.2. Characterization methods

The specific surface areas were determined by nitrogen adsorption in a Quantachrome CHEMBET3000. Before performing the adsorption, the calcined supports were treated at 400 °C for 1 h under helium flow.

Temperature programmed reduction (TPR) of the catalysts was made in a CHEMBET-3000 (QUANTACHROME Co) equipment. The experiments were carried out using 0.1 g of reduced catalyst. The sample was treated under nitrogen (10 mL/min) at 400 °C for 1 h, with a heating rate of 10 °C/min. After this, the sample was cooled down at room temperature and then a flow of 5% H_2/95% N_2 was passed through the sample. The TPR profiles were registered using a heating rate of 10 °C/min up to 500 °C with a rate flow of 10 mL/min.

High angle annular dark field (HAADF) scanning transmission electron microscopy (STEM) analysis of the samples annealed and reduced at 500 °C was performed in a JEM-2200FS, transmission electron microscope with an accelerating voltage of 200 kV. The microscope is equipped with a Schottky-type field emission gun and an ultra high resolution (UHR) configuration (Cs = 0.5 mm; Cc 1.1 mm; point-to-point resolution, 0.19 nm) and in-column omega-type energy filter.

The XPS analysis was carried out by using a THERMO VG ESCALAB 250 spectrometer equipped with an aluminum anode (energy of 1486.8 eV) and an X-ray system monochromator. The X-ray source was powered at 15 kV and 7.5 mA. In order to correct the effect of charge in the XPS spectra, all the binding energies were referenced to the C 1s line of adventitious carbon at 284.6 eV. The samples were placed on a thin sheet of indium and then analyzed. In order to control the sample charge in all the experiments, an electron flood gun was used. No additional treatment was applied to the samples prior to these measurements.

The FTIR-CO adsorption spectra were obtained at room temperature by using a FTIR Nicolet-Magna 560 apparatus, with a resolution of 2 cm^{-1} and 100 scanners. The samples pressed in thin wafers were placed in a Pyrex glass cell, equipped with CaF_2 windows, coupled to a vacuum system and gas lines supplied. The samples were maintained under vacuum (10^{-6} Torr) at 400 °C for 30 min. Then, the cell was cooled to room temperature and the CO (PRAXAIR UHP 100%) admission of 20 Torr was carried out. The CO excess was evacuated during 30 min, after this the CO adsorbed FTIR spectra were recorded.

The TPO measurements were carried out in a CHEMBET-3000 apparatus using a thermal conductivity detector (TCD), and 0.1 g of catalyst. In these experiments the flow rate of 5%O_2/95%He mixture was 10 mL/min and the heating rate was 10 °C/min. Finally, the spectra were recorded from room temperature to 500 °C.

2.3. Catalytic tests

Experiments were carried out by using a 300 mL stainless steel autoclave (Parr Instrument Co Ltd., IL, USA) equipped with a valve for sampling and a magnetic driven stirrer (set at 1000 rpm). Oxygen (10 bar) was used as oxidant source. The reaction was carried out as follows: 150 mL of an aqueous of TAME solution at a concentration of 227 ppm (corresponding to 160 ppm of C) was placed in a glass vessel to avoid the contact of the solution with the reactor and then 1 g/L of the catalyst was charged into the reactor. The reactor was firstly purged with nitrogen for 15 min and then heated at 120 °C. Afterwards, an oxygen pressure of 10 bar was introduced in the reactor and under continuous stirring (1000 rpm) the reaction was initiated. Previous calibration showed that under such conditions the reaction rate was not controlled by the diffusion of oxygen into the liquid phase. The evolution of the reaction was followed by performing the analysis of aliquots at intervals of 10 min per 1 h. The samples were collected by using the sampling valve, which is equipped with a microspore glass filter to prevent the catalyst loss. No leaching of rhodium or alumina was detected. These catalytic systems showed stability in the TAME oxidizing reaction under the CWAO conditions used in this work.

The samples were analyzed by GC with a FID detector equipped with a capillary column (DBWAX 30 m × 0.53 mm id, 1.0 μm). A temperature ramp was set up in order to separate the pollutant and their intermediates during the reaction. The analysis of total organic carbon (TOC) was performed by using a 5000TOC Shimadzu Analyzer, which was previously calibrated to obtain concentrations in the range of 0–300 ppm of TOC. TOC = after at 1 h of reaction and TOCo = value at *t* = 0.

3. Results and discussion

It was observed that the addition of cerium nitrate to boehmite leads to a diminution of the BET specific surface area of the supports from 266 $m^2\ g^{-1}$ for A to 232, 206 and 139 $m^2\ g^{-1}$ for the ACe1, ACe5 and ACe20 samples, respectively. The diminution of the specific surface areas was of the order of 6–27% for contents of 1–20 wt% Ce. This drop in the specific surface area increases with the Ce load, showing that the cerium oxide modifies the textural properties of the γ-Al_2O_3.

In Table 1 are reported the load of metals for mono metallic and bimetallic catalysts which are around 0.79–0.9 wt% for Rh and

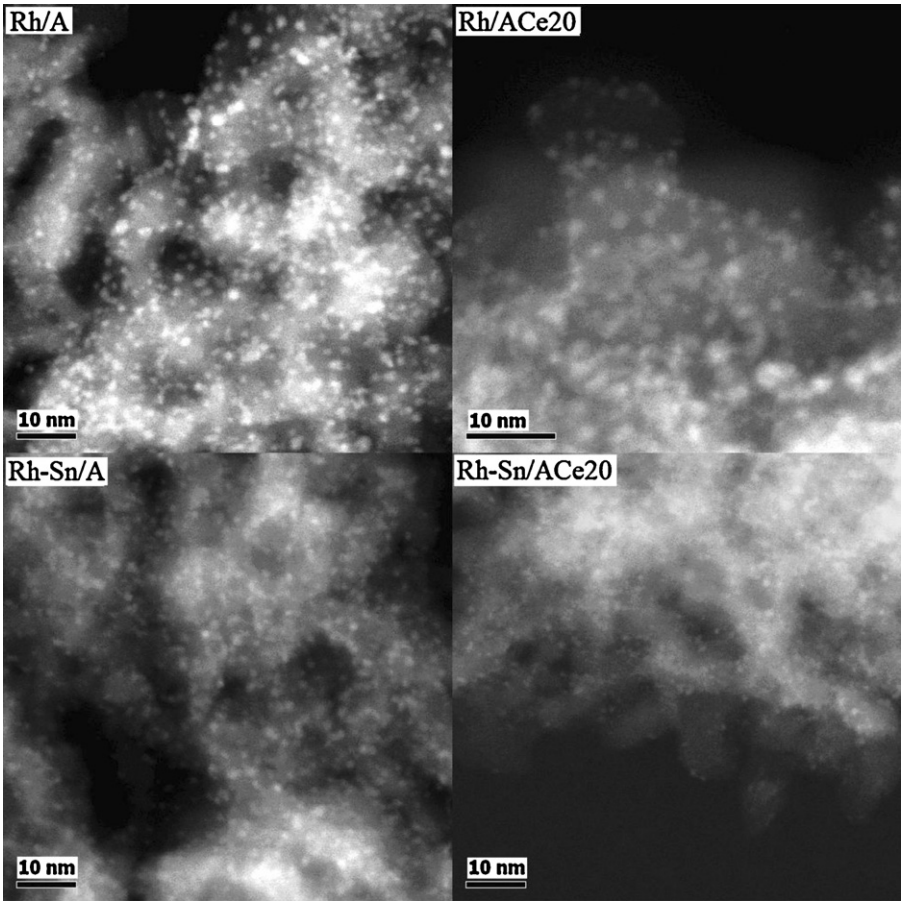

Fig. 1. HAADF-STEM images of the Rh/A, Rh/ACe20, Rh–Sn/A and Rh–Sn/ACe20 catalysts.

0.94–0.97 wt% for Sn. These values are in good agreement with the nominal percent.

The mean particle size was calculated with the expression $\phi = \Sigma n_i d_i^3 / \Sigma n_i d_i^2$, where ϕ is the mean particle size, d_i is the diameter measured directly from the electron micrographs and n_i is the number of particles having the diameter d_i. TEM micrographs exhibit a narrow distribution, for Rh monometallic catalysts particle sizes ranging from 1.0 to 2.5 nm were obtained, Table 1 and Fig. 1. The Rh–Sn bimetallic catalysts showed very small particle size at around 1.1–1.2 nm whatever the amount of ceria in the alumina supports, this result suggests that in the case of bimetallic catalysts the presence of Sn and cerium oxide trends to stabilize very small Rh particles (Fig. 1).

The H_2-TPR profiles of the catalysts are shown in Fig. 2. The Rh/A catalyst shows two reduction peaks, one at low temperature around 59 °C and the other at 154 °C. The presence of the two reduction peaks is in agreement with the reported results in the literature [23,24]. The low temperature peak is assigned to the reduction of RhOx species over the alumina surface and the other one to the RhOx species placed in the interface metal-support [25–27], Fig. 2a. For the Rh–Sn/A catalyst the high temperature peak disappears suggesting a better reducibility of the RhOx species placed in the interface metal-support caused by the presence of Sn (Fig. 2b). On Rh/ACe and Rh–Sn/ACe catalysts the profiles showed the low temperature peak around 59 and 71 °C (RhOx species) and a second one placed at temperatures comprised between 150 and 215 °C. The second peak is shifted to higher temperatures and increases with the amount of cerium oxide. Then high temperature peak can be assigned to the reduction of cerium oxide placed on the environ of the rhodium particles. Thus an assisted cerium oxide reduction by rhodium could be present. The Rh particles can indeed activate the H_2 molecules, which subsequently spillover to the CeO_2 conglomerates promoting its reduction [28,29].

The hydrogen consumption was calculated for various catalysts by integrating the low temperature peak and the values are reported in Table 2, where it can be seen that the reducibility of RhOx species presents the following order: Rh–Sn/A > Rh–Sn/ACe > Rh/ACe > Rh/A. These results showed that the presence of Sn in the catalyst increases the Rh reducibility; this behavior can be explained assuming that Sn is placed in the

Table 1
Rh content and mean particle size of Rh and Rh–Sn catalysts.

Catalyst	Rh (wt%)	ϕ[a] (nm)	Catalyst	Rh (wt%)	Sn (wt%)	ϕ[a] (nm)
Rh/A	0.79	1.1	Rh–Sn/A	0.79	0.93	1.2
Rh/ACe1	0.83	1.1	Rh–Sn/ACe1	0.85	0.96	1.2
Rh/ACe5	0.88	1.5	Rh–Sn/ACe5	0.80	0.94	1.2
Rh/ACe20	0.89	2.5	Rh–Sn/ACe20	0.90	0.97	1.1

[a] Mean particle size.

Table 2
Quantification of the TPR signals for Rh and RhSn catalysts.

Catalyst	H_2 consumption (μmol)
RhA	4.7
RhACe1	4.9
Rh/ACe5	5.3
Rh/ACe20	6.0
Rh–Sn/A	7.9
Rh–Sn/ACe1	6.5
Rh–Sn/ACe20	7.0

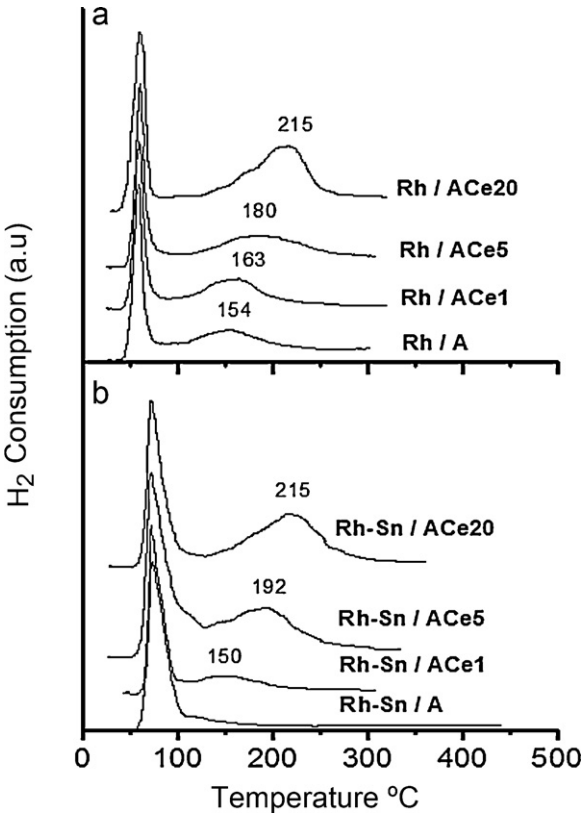

Fig. 2. H_2-TPR profiles of rhodium and rhodium–tin catalysts.

interface metal-support and consequently the Rh reducibility was increased.

The X-ray photoelectron data of Rh 3d region for some Rh monometallic catalysts are reported in Table 3. We observe that all rhodium catalysts showed reduced and oxidized species. The binding energy (BE) of Rh corresponding to the $3d_{5/2}$ core level on Rh/A catalyst shows 2 peaks one at 307.5 eV and the other at 309.0 eV corresponding to Rh° and $Rh^{\delta+}$ species. The relative proportion of these two species, calculated from the area of the deconvoluted peaks, is of 71 and 29%, respectively, Table 3. For Rh/ACe*X* catalysts the binding energies for reduced and oxidized species are around 306.9–307.5 eV and 308.4–308.9 eV, respectively. An increase of the oxidized specie with the amount of cerium oxide in the catalyst is observed.

Table 3
Binding energy of Rh $3d_{5/2}$, and Ce $3d_{5/2}$ core level and relative abundance of the different species obtained from XPS data for some Rh/Al_2O_3–CeO_2 catalysts.

Catalyst	BE (eV)		Relative abundance (%)	
	Rh $3d_{5/2}$	Ce $3d_{5/2}$	Rh°–$Rh^{\delta+}$	Ce^{3+}–Ce^{4+}
Rh/A	307.5 309.0		71–29	
Rh/ACe1	307.5 308.8	884.6 887.9 890.7 900.9	65–35	52–48
Rh/ACe5	306.9 308.4	881.9 885.3 887.6 898.7	43–57	37–63
Rh/ACe20	306.9 308.9	882.2 884.7 886.8 897.2	30–70	27–73

Fig. 3 shows the X-ray photoelectron spectra of the Rh3d and Sn3d core level for the bimetallic catalysts. For Rh–Sn/A catalyst (Table 4), the BEs for Rh° and $Rh^{\delta+}$ species were observed at 307.2 and 310.5 eV with a proportion of 60 and 40%, respectively. Besides, Sn3d core level exhibits a BE of 484.1 eV for the reduced Sn° specie and for the oxidized specie $Sn^{\delta+}$ the BE is around 485.9 eV (Sn^{2+} and Sn^{4+} species are difficult to be distinguished by XPS) [30]. In this catalyst a high proportion of reduced Sn° specie was detected (82%).

In Rh–Sn/ACe*X* catalysts (Table 4), the binding energy values corresponding to $Rh3d_{5/2}$ core level are around 307.0–307.3 eV and 308.6–309.3 eV for reduced and oxidized rhodium respectively. In those bimetallic catalysts the oxidized species $Rh^{\delta+}$ present values around 36, 38 and 68% at contents of 1, 5, and 20%Ce. Whereas $Sn^{\delta+}$ (bonding energies around 486.5–487.7 eV) specie increase with the increase of ceria, the highest relative abundance (49%) is obtained with the higher content of cerium oxide in the catalyst, Rh–Sn/ACe20. The binding energy for $Ce3d_{5/2}$ core level is also reported in Table 4, the higher proportion Ce^{4+} (886.7–899 eV) specie (67%) is obtained on Rh–Sn/ACe20 catalyst.

After these results we can conclude that the redox couples $Rh^{\circ}/Rh^{\delta+}$ and Ce^{4+}/Ce^{3+} coexist over Rh/Al_2O_3–Ce*X* catalysts, whereas, $Rh^{\circ}/Rh^{\delta+}$, Ce^{4+}/Ce^{3+} and $Sn^{\delta+}$ coexist on $Rh–Sn/Al_2O_3$–CeX catalysts.

The FTIR spectra of the CO adsorption on Rh and Rh–Sn supported on Al_2O_3 and Al_2O_3–Ce catalysts are shown in Figs. 4 and 5, respectively. The CO adsorption on Rh has been correlated with different Rh structures as well as the oxidation state of the Rh surface which depends on the Rh crystallite size and redox environment [31–34]: the bridge-bonded CO species (1850 cm^{-1}) and linearly bonded CO species (2040–2070 cm^{-1}) are formed on large Rh surface, while a geminal dicarbonyl specie (symmetric and antisymmetric bands at 2030 cm^{-1} and 2090–2100 cm^{-1}) is formed on small clusters or atomically dispersed Rh^{1+} sites [34]. In the present work, the spectra for Rh monometallic catalysts present two neighboring bands (2022 and 2091 cm^{-1}) which are clearly visible and are assigned to geminal dicarbonyl species, $Rh^{1+}(CO)_2$. The presence of gem-dicarbonyl bands in the FTIR spectra should be interpreted by the presence of Rh^{1+} ions on rhodium crystallites. Considering the high dispersion of rhodium obtained in Rh catalysts, it is assumed that CO gem-dicarbonyl form is mainly adsorbed on low coordinated sites as, i.e. corner and edges, which are electron deficient. The presence of cerium oxide does not modify the CO adsorption on Rh particles for Rh/ACe*X* catalysts (Fig. 4).

The spectra of FTIR of CO adsorption for Rh–Sn bimetallic catalysts showed also the geminal-dicarbonyl species at 2023 and 2093 cm^{-1} for symmetric and asymmetric bands, respectively. No

Table 4
Binding energy of Rh $3d_{5/2}$, Sn $3d_{5/2}$ and Ce $3d_{5/2}$ core level and relative abundance of the different species obtained from XPS data for $Rh–Sn/Al_2O_3$–CeO_2 catalysts.

Catalyst	BE (eV)			Relative abundance (%)		
	Rh $3d_{5/2}$	Sn $3d_{5/2}$	Ce $3d_{5/2}$	Rh°–$Rh^{\delta+}$	Sn°–$Sn^{\delta+}$	Ce^{3+}–Ce^{4+}
Rh–Sn/A	307.2 310.5	484.1 485.9	–	60–40	82–18	–
Rh–Sn/ACe1	307.3 308.6	484.3 487.4	885.3 889.1	64–36	66–34	100–0
Rh–Sn/ACe5	307.1 308.7	485.4 487.7	882.2 885.3 888.9 898.4	62–38	64–36	40–60
Rh–Sn/ACe20	307.0 309.3	484.9 486.5	882.0 885.0 886.7 899.0	32–68	51–49	33–67

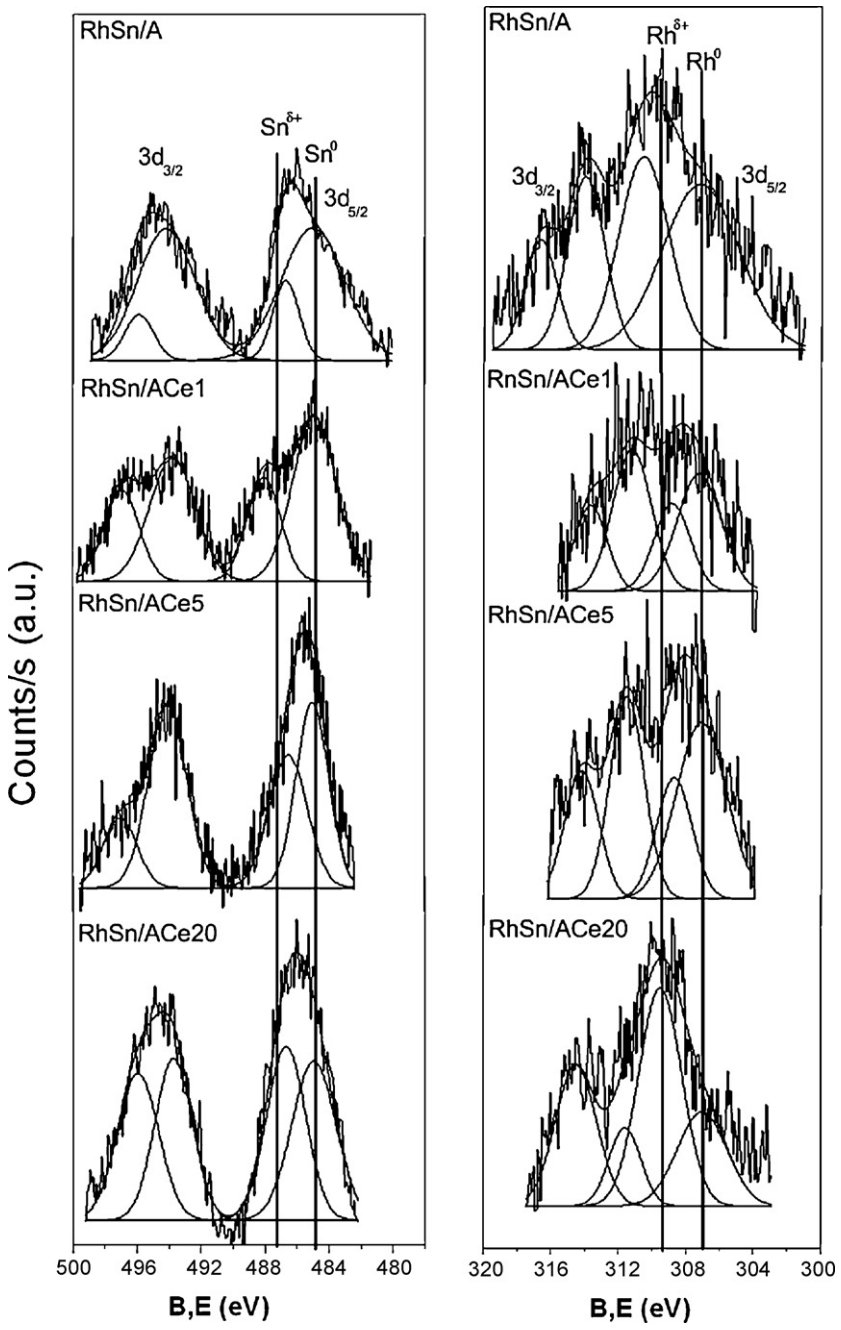

Fig. 3. XPS spectra of Rh 3d and Sn 3d core level for Rh–Sn catalysts.

additional peaks corresponding to bridged CO species (1850 cm^{-1}) or linear (2040–2070 cm^{-1}) were detected. Some studies have shown that Sn atoms will preferentially be distributed in the lowest coordination sites of Rh particles as corner and edges sites [16,17,35]. Therefore, the $Rh^{\delta+}$ sites can be diminished since Sn occupies the same sites, this explain the low intensity of the CO spectra on Rh–Sn/A catalyst (Fig. 5). On the other hand, as can be seen in Fig. 5, the relative intensities of the geminal dicarbonyl bands for bimetallic catalysts containing cerium oxide depend on the amount of cerium oxide in the catalyst. A possible interaction between SnOx–RhOx with the surrounding cerium oxide could modify the $Rh^{\delta+}$ surface sites and then the CO adsorption.

The catalytic wet air oxidation of TAME for Rh and Rh–Sn catalysts is shown in Fig. 6. The conversion of TAME as a function of time at 120 °C and 10 bar of oxygen without catalyst presents a very low transformation (~5%). It can be observed that the profile of TAME decomposition as a function of time is very similar in all the catalysts, a fast conversion of TAME in the first 10 min and a stabilization of the conversion up to 1 h of reaction.

To verify whether the molecule reactant or some intermediate molecules remain adsorbed on the catalyst, TPO determinations on the used catalysts were carried out. Fig. 7 shows the profiles of the TPO thermograms for some catalysts. A very low concentration of organic adsorbed molecules was detected, the quantitative calculation is in the range of 0.0038–0.024 mg which can be considered negligible.

In Fig. 8a and b is plotted the graphics of comparative behaviors for Rh monometallic and bimetallic catalysts for TAME conversion and TOC abatement, respectively, after 1 h of reaction. The conversion and TOC increase with the amount of cerium, then cerium

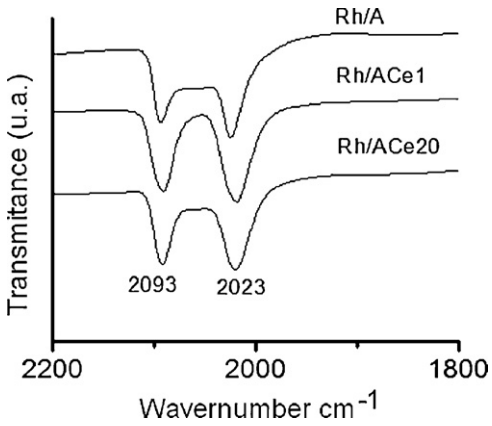

Fig. 4. FTIR spectra of CO adsorbed on Rh/A, Rh/ACe1 and Rh/ACe20 catalysts.

oxide plays an important role in the activity and total mineralization (TOC) for the TAME wet oxidation. The TPR profiles suggest a close Rh–CeO_x interaction, which can favor the reduction of cerium oxide by hydrogen spillover effect. The Rh–CeO_x interaction was also suggested by the XPS results, where the coexistence of $Rh^{\circ}/Rh^{\delta+}$ and Ce^{4+}/Ce^{3+} species in the Rh/ACe*X* catalysts is detected. Then, taking into account these findings it is proposed that on the Rh/Al_2O_3–CeO_2 catalysts, the $Rh^{\delta+}$ electron deficient particles detected by XPS are responsible of the highest activity shown by the catalysts containing cerium oxide, Fig. 8a. Due to its electron deficient character the $Rh^{\delta+}$ species activate the TAME molecules by accepting the electrons of the oxygen from the C–O–C ether function, thus promoting their cleavage and hence the increase of TAME mineralization, Fig. 8b.

In Fig. 8a and b it can be seen that addition of tin to rhodium catalysts improves the conversion and the TOC abatement. To explain these results it can be assumed that tin oxidized acts as Lewis site which can trap a molecule rich in electrons as the TAME reactant, which is placed near the active sites where the reaction occurs.

On the other hand in bimetallic Rh–Sn/ACe*X* catalyst a strong interaction between oxidized species of rhodium, tin and cerium oxide is not ruled out, where rhodium remains stabilized as $Rh^{\delta+}$. Indeed, this oxidized species were detected by FTIR-CO where only gem-dicarbonyl adsorbed species were detected on the very small Rh particles for mono and bimetallic catalysts.

These results are in agreement with TEM results which reveal a stabilization of very small rhodium particles.

It can be possible that the improvement in activity on Rh–Sn/ACe*X* catalysts comes from the $Rh^{\delta+}$ species (present in the catalysts and detected by XPS) which are close to SnO_x and CeO_x.

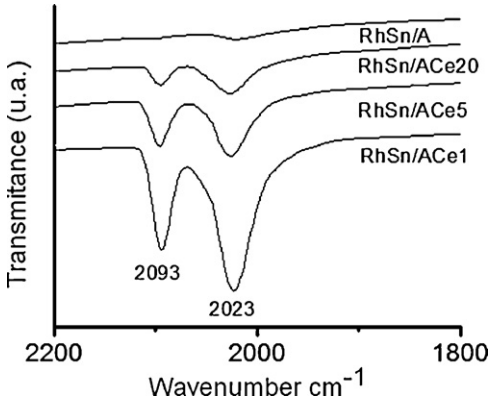

Fig. 5. FTIR spectra of CO adsorbed on Rh–Sn/A, Rh–Sn/ACe1, Rh–Sn/ACe5, Rh–Sn/ACe20 catalysts.

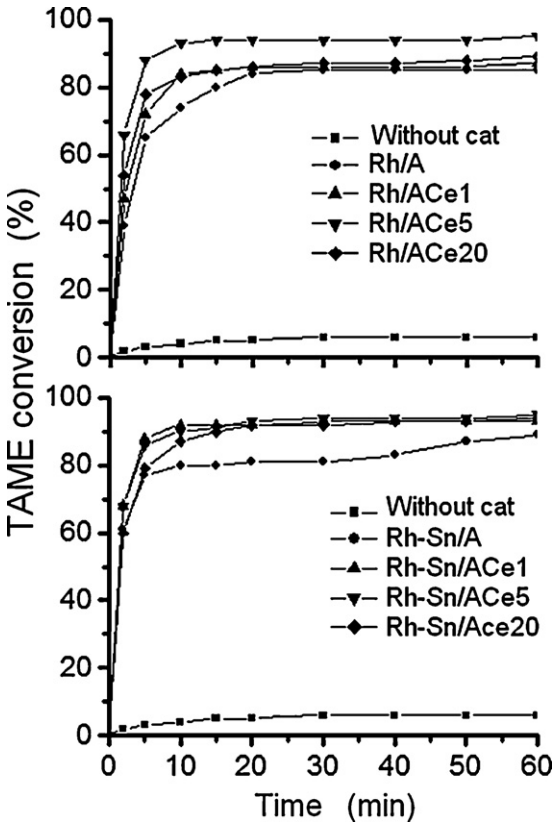

Fig. 6. TAME oxidation as a function of time for the various Rh and Rh–Sn alumina-ceria supported catalysts.

It is noticed that as the load of cerium oxide increases the relative proportion of $Sn^{\delta+}$ species augments. Therefore, an increase in the activity and especially in the TOC abatement could be attended (Fig. 8b). The higher mineralization observed on Rh–Sn/ACe catalysts (TOC) is confirmed by the important abatement in the intermediates reported in Fig. 8c.

Fig. 9 shows the typical behavior of the transformation of TAME on the Rh–Sn/ACe20 catalyst. The products detected in course of reaction were acetone, methanol, 2-methylpropene, tert-buthylalcohol. Taking into account the reaction intermediates detected, a simplified reaction scheme is presented in Fig. 10. In this scheme it is proposed that teramyl (in brackets) is the key-compound to explain the reaction pathway. This intermediate was not detected in the course of the reaction due to its reactivity. Fig. 10 shows two routs, one forming 2 methyl propene which is easily oxidized towards total mineralization, the other route form-

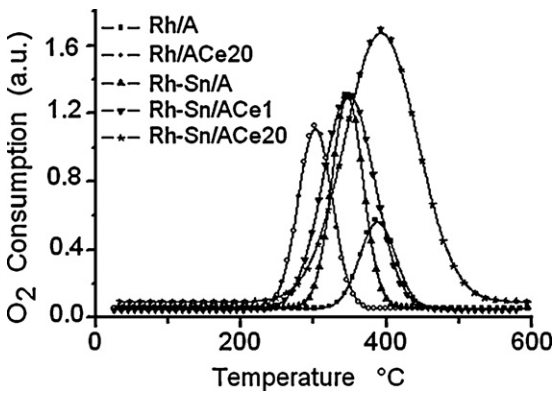

Fig. 7. TPO thermograms for used Rh and Rh–Sn alumina-ceria supported catalysts.

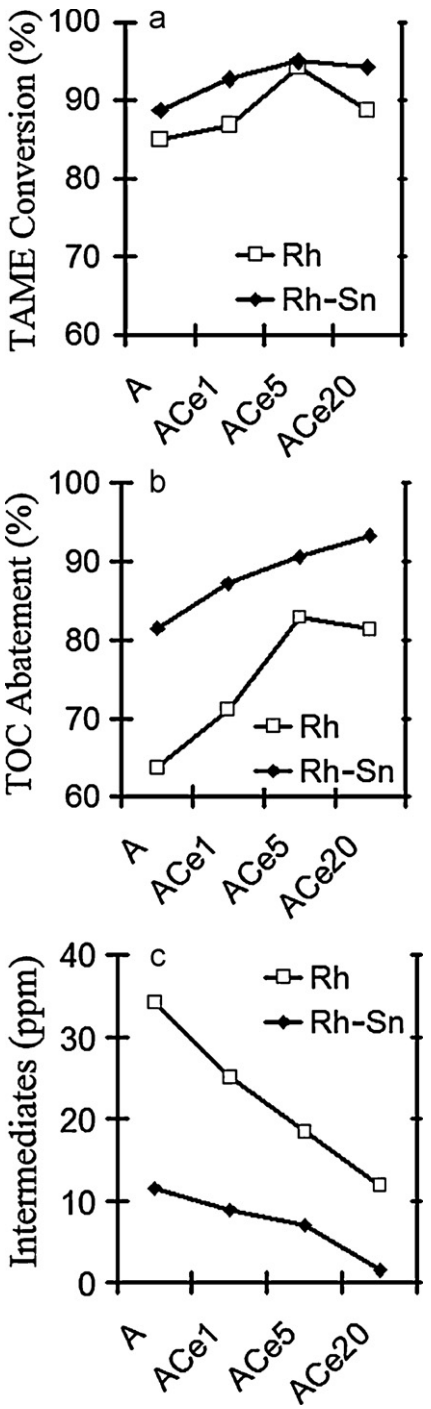

Fig. 8. Comparative behavior for Rh/ACeX and Rh–Sn/ACeX catalysts on TAME conversion, TOC abatement, and intermediates formation.

ing terbutanol and subsequently acetone and finally total oxidation to obtain $CO_2 + H_2O$.

4. Conclusions

Very small rhodium particles were obtained on $Rh/Al_2O_3–CeO_2$ and $Rh–Sn/Al_2O_3–CeO_2$ catalysts. It was detected by XPS that the addition of cerium oxide to rhodium alumina supported catalysts favors the formation of $Rh^{\circ}/Rh^{\delta+}$ and Ce^{4+}/Ce^{3+} redox couples. An improvement in the TOC abatement was obtained for CWAO of TAME by the effect of cerium oxide. It showed that the presence

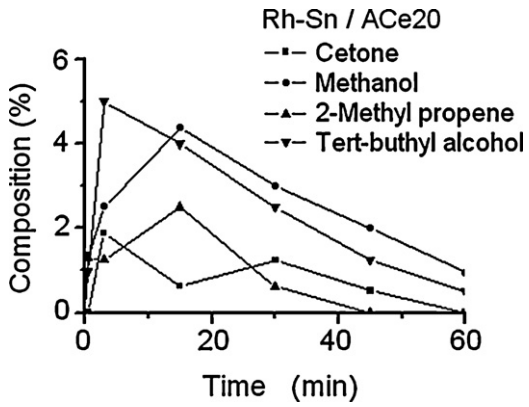

Fig. 9. Evolution of TAME oxidation intermediates as a function of time on Rh–Sn/ACe20 catalyst.

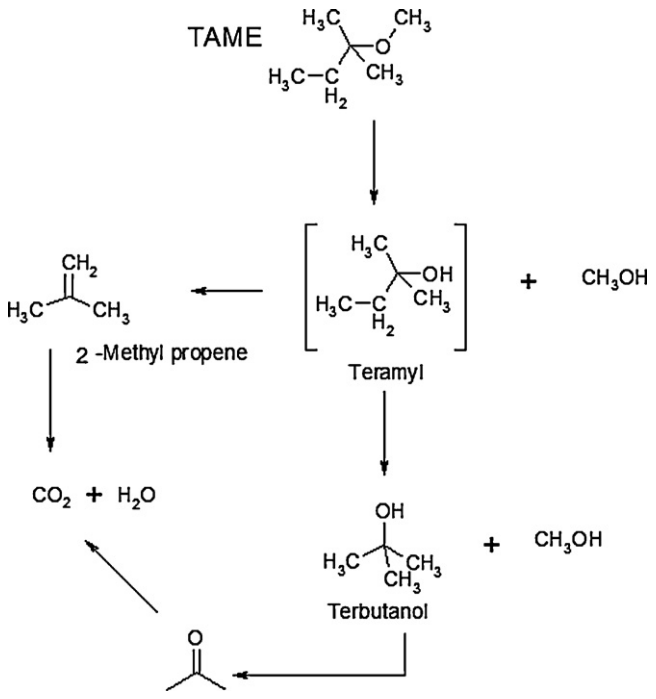

Fig. 10. Proposal reaction pathway for the TAME wet oxidation.

of $Sn^{\delta+}$ species in the Rh–Sn/ACeX catalysts improves notably the TAME mineralization.

Acknowledgements

We acknowledge CONACYT for the support provided to the Project 33567E.

References

[1] R.D. White, W.C. Doughtrey, M.S. Wells, Toxicol. Lett. 82/83 (1995) 719.
[2] A.A. Urbano, D.D. Dinoysiou, M.T. Suidan, T.L. Richardson, Water Res. 39 (2009) 107.
[3] B. Neppolian, H. Hung, H. Choi, J.H. Lee, J.W. Kang, Water Res. 36 (2002) 4699.
[4] J. Barbier Jr., F. Delanoe, F.J. Jabouille, D. Duprez, G. Blanchard, P. Isnard, J. Catal. 177 (1998) 378.
[5] S. Imamura, H. Kinunaka, N. Kawabata, Ind. Eng. Chem. Res. 27 (1988) 718.
[6] Z.P.G. Masende, B.F.M. Kruster, K.J. Ptasinski, F.J.J.G. Jansen, J.H.Y. Katima, J.C. Schouten, Top. Catal. 33 (1–4) (2005) 101.
[7] S.C. Kim, B.Y. Jeong, D.K. Lee, Top. Catal. 33 (1–4) (2005) 149.
[8] M. Beson, Gallezot., Top. Catal. 33 (1–4) (2005) 101.
[9] J.M. Beziat, M. Besson, P. Gallezot, S. Durecu, J. Catal. 182 (1999) 129.

[10] D.K. Lee, D.S. Kim, Catal. Today 63 (2–4) (2000) 249.
[11] J. Barbier Jr., L. Oliviero, B. Renard, D. Duprez, Catal. Today 75 (1–4) (2002) 29.
[12] E. Castillejos-López, A. Maroto-Valiente, D.M. Nevskaia, V. Muñoz, I. Rodríguez-Ramos, A. Guerrero-Ruiz, Catal. Today 143 (3/4) (2009) 355.
[13] H.T. Gomes, J.J.M. Orfao, J.L. Figueiredo, J.L. Faria, Ind. Eng. Chem. Res. 43 (5) (2004) 1216.
[14] B. Levasseur, B. Renard, J. Barbier Jr., D. Duprez, React. Kinet. Catal. Lett. 87 (2) (2006) 269.
[15] S.H. Hosokawa, H. Kanai, K. Utani, Y. Taniguchi, Y. Saito, S. Imamura, Appl. Catal. B: Environ. 45 (2003) 181.
[16] J.P. Candy, B. Didillon, E.L. Smith, T.B. Shay, J.M. Basset, J. Mol. Catal. 86 (1994) 179.
[17] B. Coq, F. Figueras, Coord. Chem. Rev. 178–180 (1998) 1753.
[18] J.L. Margitfalvi, G. Vanko, I. Borbath, A. Thompos, A. Vertes, J. Catal. 190 (2000) 474.
[19] C.G. Raab, J.A. Lercher, J. Mol. Catal. 75 (1992) 71.
[20] I. Cuauhtemoc, G. Del Angel, G. Torres, J. Navarrete, C. Angeles-Chavez, J.M. Padilla, J. Ceram. Proc. Res. 10 (4) (2009) 512.
[21] L. Basini, D. Sanfilippo, J. Catal. 157 (1995) 162.
[22] H.Y. Wang, E. Ruckenstein, Appl. Catal. A 204 (2000) 143.
[23] W.Z. Weng, X.Q. Dei, J.M. Li, H.Q. Lin, Ch.J. Huang, H.L. Wan, Catal. Today 117 (2006) 53.
[24] C.P. Hwang, C.T. Yeh, Q. Zhu, Catal. Today 51 (1999) 93.
[25] P. Fornasiero, R. Di Monte, G.R. Rao, J. Kaspar, S. Meriani, A. Trovarelli, M. Graziani, J. Catal. 151 (1995) 168.
[26] J.C. Vis, H.F.J. Vant Blink, T. Huizinga, J. Van Grondelle, R.J. Prins, J. Catal. 95 (1985) 95.
[27] R. Wang, H. Xu, X. Liu, Q. Ge, W. Li, Appl. Catal. A: Gen. 305 (2006) 204.
[28] A. Trovareli, C. de Leitenburg, G. Dolcetti, J.L. Lorca, J. Catal. 151 (1995) 111.
[29] S. Bernal, J.J. Calvino, G.A. Cifredo, J.M. Rodriguez-Izquierdo, V. Pericón, A. Laachir, J. Catal. 137 (1992) 1.
[30] M.C. Aguirre, P. Reyes, M. Oportos, I. Melian-Cabrera, J.L.G. Fierro, Appl. Catal. A: Gen. 233 (2002) 183.
[31] A.C. Yang, G.W. Garland, J. Phys. Chem. 61 (1957) 1504.
[32] F. Solymosi, M. Pasztor, J. Phys. Chem. 90 (1986) 5312.
[33] R. Dictor, S. Roberts, J. Phys. Chem. 93 (1989) 2526.
[34] G. Lafaye, C. Mihut, C. Special, P. Marecot, M.D. Amiridis, Langmuir 20 (2004) 10612.
[35] B. Coq, A. Goursot, T. Tazi, F. Figueras, D.R. Salahub, J. Am. Chem. Soc. 113 (1991) 1485.